RSC Advances

RSC Publishing

PAPER

Preparation of Zn–Co–O mixed-metal oxides nanoparticles through a facile coordination polymer based process†

Cite this: *RSC Advances*, 2013, **3**, 4081

Jiao Zhao,[a] Yuliang Zhang,[ab] Panpan Su,[ab] Zongxuan Jiang,[a] Qihua Yang*[a] and Can Li*[a]

Received 15th November 2012,
Accepted 17th January 2013

DOI: 10.1039/c3ra22913k

www.rsc.org/advances

This paper reports a facile process that starts from the coordination polymers (CPs) precursor for the preparation of mixed-metal oxides. Firstly, a series of CPs, Zn–Co–ptcda (ptcda = perylene-3,4,9,10-tetracarboxylic dianhydride) with different molar ratios of Zn^{2+} and Co^{2+}, were prepared by self-assembly of metal ions and organic ligands at the molecular scale. Based on the scanning electron microscopy, X-ray diffraction and thermogravimetric analysis, Zn–Co–ptcda takes both the advantages of Zn–ptcda and Co–ptcda. After a simple thermal treatment, the mixed-metal CPs are transformed into mixed-metal oxides with morphology and composition inherited from the CPs precursor. Binary-phase oxide Co_3O_4/ZnO and single-phase spinel $Zn_xCo_{3-x}O_4$ ($0 < x < 1$) can be successfully prepared by this strategy.

Introduction

Metal oxide nanomaterials have triggered much research activity because of their wide applications in the fields of magnetics, microelectronics, optics, catalysis, and so on.[1–5] In particular, the mixed-metal oxides, which contain more than two metal oxides within a nanoscale particle, have received a great deal of attention as they display modified properties and have been proposed as candidates for multifunctional materials.[6–10] Mixed-metal oxides have been widely used as active catalysts for the dehydrogenation of alcohols, the selective hydrogenation and isomerization of olefins, the water-gas shift reaction, the photocatalytic water splitting, *etc*.[11–15] For example, the mixed-metal oxides have shown superior performance for removing thiophenic sulfur compounds from liquid fuels.[16]

Many synthetic methods have been described to produce mixed-metal oxides, such as mechanical mixing, spray pyrolysis, sol–gel, hydrothermal, and polymer-based processes.[17–19] In comparison with the single metal oxides, the preparation of the solid solution like mixed-metal oxides is challenging because the stoichiometry and homogeneity of different compositions should be considered in addition to the crystalline phase, the morphology and the particle size.[20–23] Thus, it still lacks a general preparation method for the mixed-metal oxides with tunable chemical compositions and homogeneous distribution. Recently, our group and others have reported that coordination polymers (CPs) built from metal ions and organic bridging ligands could be easily transformed into metal oxides.[24–32] Through a simple thermal treatment in air, the organic part of the CPs could be easily removed, and the metal oxides with morphology inherited from the CPs could be facilely fabricated. The morphology and composition can be controlled step by step, so that the size, morphology, structure, and property of the metal oxides can be tuned. However, the thermal transformation of CPs to metal oxides mainly focused on single-metal oxides, the preparation of mixed-metal oxides using this method is seldom reported.[33–35]

In this paper, we report the synthesis of mixed-metal oxide nanoparticles with well-defined micro-plate morphology using mixed-metal CPs, Zn–Co–ptcda (ptcda = perylene-3,4,9,10-tetracarboxylic dianhydride) as precursor, followed by a simple thermal treatment process. The CPs with mixed metal ions coordinated with the organic ligands have uniform distribution of metal ions at atomic-scale. Therefore, the physical and chemical properties of CPs could be finely tuned by varying the molar ratio of metal ions. More importantly, the CPs could be transformed into mixed-metal oxides by thermal treatment. The uniform distribution of metal ions at atomic-scale favors the formation of high quality mixed-metal oxides with morphology and composition inherited from the CPs precursors. We provide a systematic research and demonstrate the efficiency of this strategy for the synthesis of mixed-metal oxides, single-phase spinel $Zn_xCo_{3-x}O_4$ ($0 < x < 1$) and binary-

[a]*State Key Laboratory of Catalysis, Dalian Institute of Chemical Physics, Chinese Academy of Sciences, 457 Zhongshan Road, Dalian, 116023, P. R. China. E-mail: yangqh@dicp.ac.cn; canli@dicp.ac.cn; Fax: 86-411-84694447; Tel: 86-411-84379552 Tel: 86-411-84379070*

[b]*Graduate School of the Chinese Academy of Sciences, Beijing 100049, P. R. China*

† Electronic supplementary information (ESI) available: Full information about SEM images, EDX spectra, TG profiles. See DOI: 10.1039/c3ra22913k

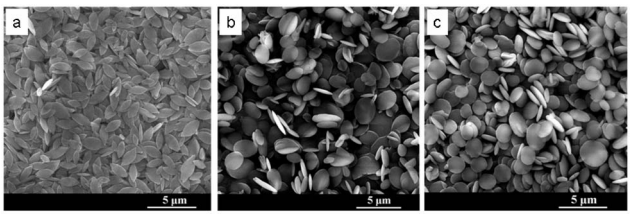

Fig. 1 SEM images of Zn–Co–ptcda CPs with different Zn/Co molar ratios: (a) Zn/Co = 3/1, (b) Zn/Co = 1/1, and (c) Zn/Co = 1/3.

phase Co_3O_4/ZnO mixed oxides, with well-defined composition and morphology.

Results and discussion

Zn–ptcda has rhombus lamella particles with particle size of 15 × 5 × 0.5 μm, and Co–ptcda shows ellipsoid-like morphology with particle size of 1.6 × 1.4 × 0.5 μm as we previously reported (Fig. S1, ESI†).[32] The scanning electron microscopy (SEM) images of Zn–Co–ptcda-*n* with different Zn/Co molar ratios are shown in Fig. 1. Uniform rhombus lamella particles with particle size of about 2.5 × 1 × 0.35 μm are the main products of Zn–Co–ptcda-3 with Zn/Co molar ratio of 3/1. This means that the coordination of Co ions in Zn–ptcda results in the decrease of particle size. With further reducing Zn/Co molar ratio to 1/1, round-plate like particles are observed in the SEM image of Zn–Co–ptcda-1, similar to Co–ptcda. Zn–Co–ptcda-0.33 (Zn/Co = 1/3) also has the round-plate like morphology. Zn–Co–ptcda-1 and Zn–Co–ptcda-0.33 have similar particle size of 2.5 × 2 × 0.35 μm, which is relatively larger than that of Co–ptcda. Based on the SEM characterization, it can be concluded that Zn–Co–ptcda-*n* with Zn/Co ratio >1 and ⩽1, has similar morphology to Zn–ptcda and Co–ptcda, respectively.

Energy-dispersive X-ray spectroscopy (EDX) analysis shows the expected zinc and cobalt signals, confirmed the existent of zinc and cobalt elements in the mixed-metal Zn–Co–ptcda-*n* CPs (Fig. S2, ESI†). Taken Zn–Co–ptcda-1 as a typical example, the distribution of elements is clarified by the EDX mapping, which reveals that zinc and cobalt elements are homogeneously distributed in the whole sample (Fig. 2a). The transmission electron microscopy (TEM) observation and selected area electron diffraction (SAED) analysis of an isolated particle display single crystal property with periodic diffraction spots (Fig. 2b). Furthermore, element distribution analysis on the selected nano-region shows the similarity of the zinc and cobalt composition, which proves that both elements are distributed homogeneously in the Zn–Co–ptcda-1 particle (Fig. 2c). The above results show that Zn–Co–ptcda-1 is single-crystalline with homogeneous distribution of different metal ions.

The powder X-ray diffraction (PXRD) patterns of Zn–Co–ptcda-*n* as well as Zn–ptcda and Co–ptcda show strong diffraction peaks at similar positions, indicating that all CPs are isostructural (Fig. 3A). All samples have {00h} crystallographic texture structure with orthorhombic crystal system and *Pbam* space group, the same as Zn–ptcda of our previous report.[32] For orthorhombic crystals, the lattice parameter *c* is related to the crystal data of {00h} crystal planes, so the variation of *d* values of (003) crystal plane with the different Zn/Co molar ratios is given, as shown in Fig. 3B. Zn–ptcda has the largest d_{003} value. The diffraction peaks of {00h} shifts gradually to higher position with the Co content increasing, thus the d_{003} decreases gradually. The above results reveal that the lattice parameter *c* decreases with the molar ratio of Co increasing. The Co content plays a role in the variation of lattice parameters that gives an indication for the Co substituting in the Zn–ptcda crystalline structure since the ionic radius of Co^{2+} (0.58 Å) is less than that of Zn^{2+} (0.60 Å).[20]

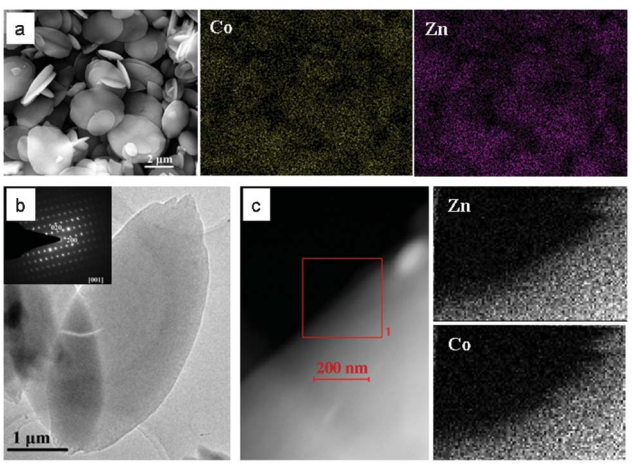

Fig. 2 (a) SEM image of Zn–Co–ptcda-1 and elemental mapping of Zn and Co. (b) TEM image of an isolated Zn–Co–ptcda-1 particle, inset is the SAED pattern. (c) STEM image of a selected nano-region of Zn–Co–ptcda-1 particle and the elemental mapping of Zn and Co.

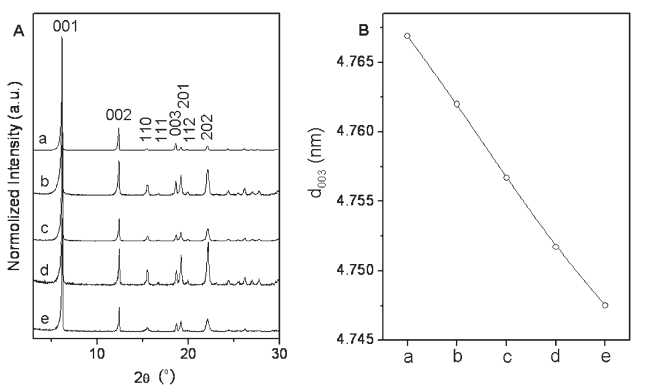

Fig. 3 (A) XRD patterns and (B) d_{003} for (a) Zn–ptcda, (e) Co–ptcda, and Zn–Co–ptcda-*n* with different Zn/Co molar ratios (b) Zn/Co = 3/1, (c) Zn/Co = 1/1, and (d) Zn/Co = 1/3.

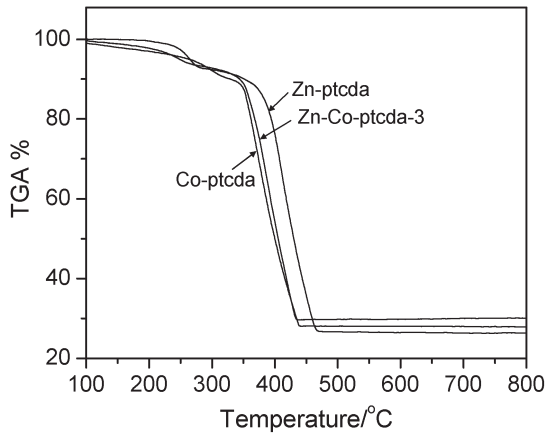

Fig. 4 TG profiles of Zn–ptcda, Co–ptcda, and Zn–Co–ptcda-3.

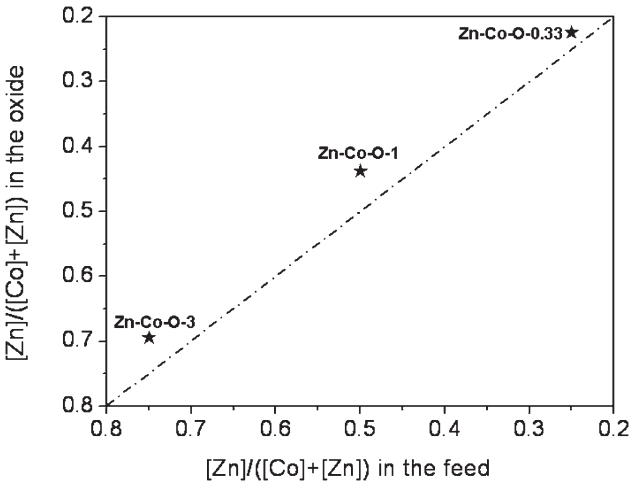

Fig. 5 Ratio of Zn content to whole metal content in feed *versus* that determined in the mixed-metal oxides by means of ICP-AES (The dash line shows the nominal composition).

The thermal stability of the mixed-metal CPs, Zn–Co–ptcda-*n*, as well as Zn–ptcda and Co–ptcda has been investigated by TG analysis, as shown in Fig. 4 and Fig. S3, ESI†. It is found that Zn–ptcda and Co–ptcda is stable up to 370 °C and 347 °C, respectively. Above those temperatures, there is a well-defined weight loss due to the escape of perylene by decarboxylation.[32] The coordination ability of different metal ions can be estimated from the decarboxylation temperature of M–ptcda CPs, since the stronger coordination bond of metal and carboxylate will make the decarboxylation easier. As the decarboxylation temperature of Zn–ptcda is higher than that of Co–ptcda, the coordination ability is in the order of Zn < Co. As for the mixed-metal CPs, the decarboxylation temperature of Zn–Co–ptcda-3 is lower than that of Zn–ptcda while a little higher than that of Co–ptcda. Zn–Co–ptcda-1 and Zn–Co–ptcda-0.33 both has similar thermal-decomposition behavior as Co–ptcda. The thermal stability of Zn–Co–ptcda-*n* is between that of Zn–ptcda and Co–ptcda, which is close to Co–ptcda. The above results suggest that the presence of Co^{2+} makes the decomposition of M–ptcda CPs easier.

Mixed-metal CPs, Zn–Co–ptcda-*n*, could be converted into mixed-metal oxides Zn–Co–O-*n* by thermal treatment in air with the organic portion escaping. The resulting Zn–Co–O materials have a composition pre-defined by the zinc content to the overall metal content ratio in the initial reactants as shown in Fig. 5. It should be pointed out that the Zn content in the final Zn–Co–O mixed-metal oxides is systematically smaller than the nominal composition according to the initial reactants, which may be related to the weaker coordination ability of Zn^{2+} than Co^{2+} based on the TG analysis. During the mixed-metal CPs formation process in this system, Co^{2+} is relatively easier to coordinate with ptcda ligand, thus, more Co^{2+} can get into the mixed-metal CPs and then into the final mixed-metal oxides.

As shown in the SEM images in Fig. 6, the resulting mixed-metal oxides Zn–Co–O materials maintain the morphology of corresponding CPs precursors, however, the particle sizes decrease due to the large volume shrinkage after the escape of perylene by thermal treatment. Uniform rhombus lamella particles and round-plate like particles are obtained for Zn–Co–O-3 and Zn–Co–O-1 (0.33), respectively. The chemical compositions of the resulting mixed-metal oxides were determined using EDX spectroscopy, in which Zn and Co elements were observed (Fig. S4, ESI†).

Fig. 7 shows the PXRD patterns of the mixed-metal oxide products covering the whole composition range. For Zn–Co–O-3, the main phase is wurtzite structured ZnO with a secondary phase Co_3O_4 observed. Clear indications for segregation into wurtzite structure of ZnO and spinel structure of Co_3O_4 are found for sample Zn–Co–O-1. The appearance of reflections in the XRD patterns belonging to two different phases indicates that mixed-metal oxides with different phase structure and elemental composition have been formed inside one particle. For Zn–Co–O-0.33, all the measured reflections can be assigned to spinel structure Co_3O_4 phase without ZnO phase. Co_3O_4 takes a cubic spinel structure with Co^{2+} and Co^{3+} located at tetrahedral and octahedral sites, respectively. This clearly indicates that zinc is well incorporated into the Co_3O_4 lattice without phase segregation, forming $Zn_xCo_{3-x}O_4$ ($0 < x < 1$) with the replacement of Co^{2+} by Zn^{2+}. In contrast, the sample prepared from a mixture of Zn–ptcda and Co–ptcda

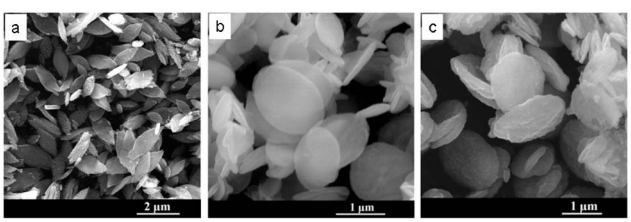

Fig. 6 SEM images of mixed-metal oxides produced from Zn–Co–ptcda CPs with different Zn/Co content ratios: (a) Zn/Co = 3/1, (b) Zn/Co = 1/1, and (c) Zn/Co = 1/3.

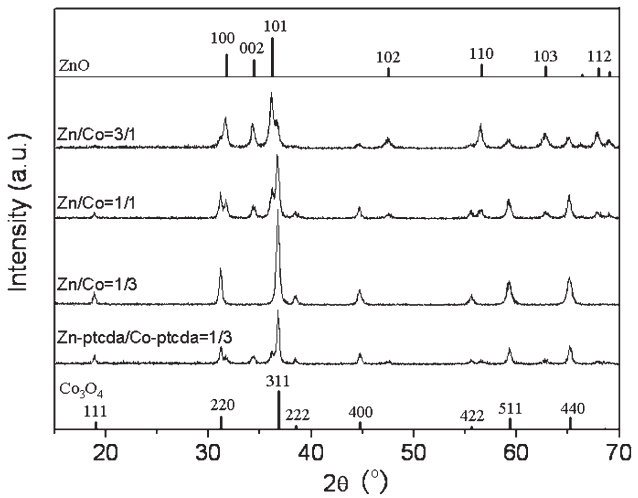

Fig. 7 PXRD patterns of the mixed-metal oxides Zn–Co–O produced from Zn–Co–ptcda CPs with different Zn/Co content ratios: 3/1, 1/1, 1/3, and mixture of Zn–ptcda and Co–ptcda CPs with Zn/Co molar ratio of 1/3. The short tick marks give the positions of standard reflections of ZnO and Co_3O_4 with JCPDS no. 89-0510 and 73-1701 respectively.

CPs with Zn/Co molar ratio of 1/3 shows clear (002) reflection of ZnO.

Fig. 8 shows the HRTEM images of the mixed-metal oxides with Zn/Co molar ratio of 1/1 and 1/3. As shown in Fig. 8a, the mixed-metal oxides are composed of nanoplates with particle size of *ca.* 20 nm. Analysis of the lattice fringe image of Zn–Co–O-1 is consistent with a calculated planar space of 0.47 nm in the (111) plane of the spinel Co_3O_4; 0.25 and 0.28 nm in the (101) and (100) planes, respectively, of the hexagonal wurtzite ZnO (Fig. 8b). This clearly indicates that the resulting mixed-metal oxides are composed of numerous ZnO and Co_3O_4 nanocrystal hybrids at nanoscale inside one particle. Consequently, the distribution of Zn and Co in the EDX elemental mapping is different because of the phase separation (Fig. 8c). For Zn–Co–O-0.33, analysis of the lattice fringe image is consistent with a calculated planar space of 0.47 nm in the (111) plane of the spinel Co_3O_4 (Fig. 8d), coinciding with the PXRD results. The similarity of the EDX elemental mapping of Zn and Co composition proves that both elements are homogeneously distributed over the whole particle (Fig. 8e).

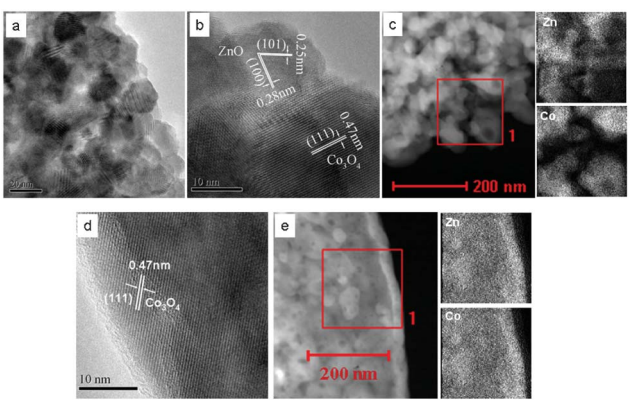

Fig. 8 HRTEM images (a, b, d) and STEM images and elemental mapping data (c, e) for (a, b, c) Zn–Co–O-1 and (d, e) Zn–Co–O-0.33.

Based on the above characterization, it can be concluded that mixed-metal oxides and spinel structured nanoparticles could be controllably formed by adjusting the initial molar ratio of metal ions in the CPs precursor. The detailed formation mechanism is not very clear. We think that it is probably related with the difference in coordination ability and metal ion radius between Zn and Co.

Conclusion

In summary, we have developed a simple coordination polymers based method to prepare mixed-metal oxide, Zn–Co–O nanomaterials. Mixed-metal CPs precursors, Zn–Co–ptcda-*n* with different Zn/Co molar ratios, have been synthesized with homogeneous distribution of two different metal ions firstly. Then, after a thermal treatment process, morphology and composition inherited mixed-metal oxides, Zn–Co–O-*n*, Co_3O_4/ZnO hybrid materials and spinel $Zn_xCo_{3-x}O_4$, have been obtained. This work offers possibilities for the development of new functional materials. Since a wide range of metal ions can be used to prepare the mixed-metal CPs precursors, this approach will be general and worthy to design and create mixed-metal oxide multifunctional systems.

Experimental methods

Synthesis of Zn–Co–ptcda CPs with different Zn/Co molar ratios

In a typical synthesis,[32] 0.2 mmol $Zn(OAc)_2{\cdot}2H_2O$ and 0.2 mmol $Co(OAc)_2{\cdot}4H_2O$ were dissolved in 22.5 mL deionized water; and 0.2 mmol ptcda was dissolved in 12.5 mL NaOH solution (0.8 mmol NaOH). The ptcda solution was added dropwise to metal acetate solution with stirring. Immediate formation of precipitate was observed. The reaction mixture was stirred at room temperature for 30 min, and then transferred into a Teflon-lined stainless steel vessel (45 mL) and heated at 100 °C for 24 h. After cooling down to room temperature, the precipitate was collected by centrifugation and washed several times with water. The obtained sample was denoted as Zn–Co–ptcda-1. The samples synthesized under similar conditions but with different Zn/Co molar ratios were denoted as Zn–Co–ptcda-*n*, where *n* (*n* = 3, and 0.33) is the Zn/Co molar ratio.

Transformation of Zn–Co–ptcda into Zn–Co–O nanomaterials

In a typical process, Zn–Co–ptcda-*n* CPs were thermally treated in air at 550 °C for 1 h with a ramp of 5 °C min^{-1}. The obtained samples were denoted as Zn–Co–O-*n*, where *n* (*n* = 3, 1, and 0.33) is the Zn/Co molar ratio of Zn–Co–ptcda precursors.

Characterization

The thermogravimetric (TG) analysis was performed under air atmosphere with a heating rate of 5 °C min^{-1} by using a NETZSCH STA-449F3 thermogravimetric analyzer. The powder X-ray diffraction data (PXRD) were collected on a Rigaku D/Max2500PC diffractometer with Cu-Kα radiation (λ = 1.5418 Å) over the 2θ range of 3°–70° with a scan speed of 5° min^{-1} at room temperature. Scanning electron microscopy (SEM) was undertaken on a JEOL JSM-6360 scanning electron microscope operating at an acceleration voltage of 20 kV. The samples were sputtered with gold prior to imaging. Selected-area electron-diffraction (SAED) and high-resolution transmission electron microscopy (HRTEM) images were recorded on a FEI Tecnai F30 microscope with a point resolution of 0.20 nm operated at 300 kV. The metal content was determined by PLASAM-SPEC-II inductively coupled plasma atomic emission spectrometry (ICP).

Acknowledgements

This work was supported by the Program Strategic Scientific Alliances between China and The Netherlands (Grant 2008DFB50130) and the National Basic Research Program of China (Grant 2009CB623503).

References

1 I. S. Lee, N. Lee, J. Park, B. H. Kim, Y. W. Yi, T. Kim, T. K. Kim, I. H. Lee, S. R. Paik and T. Hyeon, *J. Am. Chem. Soc.*, 2006, **128**, 10658.
2 K. T. Nam, D. W. Kim, P. J. Yoo, C. Y. Chiang, N. Meethong, P. T. Hammond, Y. M. Chiang and A. M. Belcher, *Science*, 2006, **312**, 885.
3 H. M. Xiong, Y. Xu, O. G. Ren and Y. Y. Xia, *J. Am. Chem. Soc.*, 2008, **130**, 7522.
4 F. Jiao and H. Frei, *Angew. Chem., Int. Ed.*, 2009, **48**, 1841.
5 J. H. Lee, Y. M. Huh, Y. Jun, J. Seo, J. Jang, H. T. Song, S. Kim, E. J. Cho, H. G. Yoon, J. S. Suh and J. Cheon, *Nat. Med.*, 2007, **13**, 95.
6 H. J. Fan, M. Knez, R. Scholz, K. Nielsch, E. Pippel, D. Hesse, M. Zacharias and U. Gosele, *Nat. Mater.*, 2006, **5**, 627.
7 M. T. Klem, D. A. Resnick, K. Gilmore, M. Young, Y. U. Idzerda and T. Douglas, *J. Am. Chem. Soc.*, 2007, **129**, 197.
8 O. Bondarchuk, X. Huang, J. Kim, B. D. Kay, L. S. Wang, J. M. White and Z. Dohnalek, *Angew. Chem., Int. Ed.*, 2006, **45**, 4786.
9 J. B. Park, J. Graciani, J. Evans, D. Stacchiola, S. D. Senanayake, L. Barrio, P. Liu, J. F. Sanz, J. Hrbek and J. A. Rodriguez, *J. Am. Chem. Soc.*, 2010, **132**, 356.
10 J. A. Rodriguez and D. Stacchiola, *Phys. Chem. Chem. Phys.*, 2010, **12**, 9557.
11 S. Surnev, M. G. Ramsey and F. P. Netzer, *Prog. Surf. Sci.*, 2003, **73**, 117.
12 I. Muylaert and P. Van Der Voort, *Phys. Chem. Chem. Phys.*, 2009, **11**, 2826.
13 I. E. Wachs and B. M. Weckhuysen, *Appl. Catal., A*, 1997, **157**, 67.
14 L. G. Tejuca, J. L. G. Fierro and J. M. D. Tascon, *Adv. Catal.*, 1989, **36**, 237.
15 B. J. Ma, J. H. Yang, H. X. Han, J. T. Wang, X. H. Zhang and C. Li, *J. Phys. Chem. C*, 2010, **114**, 12818.
16 Y. L. Zhang, Y. X. Yang, H. X. Han, M. Yang, L. Wang, Y. N. Zhang, Z. X. Jiang and C. Li, *Appl. Catal., B*, 2012, **119–120**, 13.
17 J. Marchal, T. John, R. Baranwal, T. Hinklin and R. M. Laine, *Chem. Mater.*, 2004, **16**, 822.
18 M. Kakihana, T. Okubo, M. Arima, O. Uchiyama, M. Yashima, M. Yoshimura and Y. Nakamura, *Chem. Mater.*, 1997, **9**, 451.
19 A. Sin and P. Odier, *Adv. Mater.*, 2000, **12**, 649.
20 I. Balti, A. Mezni, A. Dakhlaoui-Omrani, P. Leone, B. Viana, O. Brinza, L. S. Smiri and N. Jouini, *J. Phys. Chem. C*, 2011, **115**, 15758.
21 G. Q. Lu, I. Lieberwirth and G. Wegner, *J. Am. Chem. Soc.*, 2006, **128**, 15445.
22 E. R. Leite, A. P. Maciel, I. T. Weber, P. N. Lisboa, E. Longo, C. O. Paiva-Santos, A. V. C. Andrade, C. A. Pakoscimas, Y. Maniette and W. H. Schreiner, *Adv. Mater.*, 2002, **14**, 905.
23 N. L. Wu, S. Y. Wang and I. A. Rusakova, *Science*, 1999, **285**, 1375.
24 W. Cho, Y. H. Lee, H. J. Lee and M. Oh, *Chem. Commun.*, 2009, 4756.
25 W. Cho, S. Park and M. Oh, *Chem. Commun.*, 2011, **47**, 4138.
26 S. Jung, W. Cho, H. J. Lee and M. Oh, *Angew. Chem., Int. Ed.*, 2009, **48**, 1459.
27 W. Cho, Y. H. Lee, H. J. Lee and M. Oh, *Adv. Mater.*, 2011, **23**, 1720.
28 C. C. Li, X. M. Yin, L. B. Chen, Q. H. Li and T. H. Wang, *Chem.–Eur. J.*, 2010, **16**, 5215.
29 B. Liu, X. B. Zhang, H. Shioyama, T. Mukai, T. Sakai and Q. Xu, *J. Power Sources*, 2010, **195**, 857.
30 H. Y. Shi, B. Deng, S. L. Zhong, L. Wang and A. W. Xu, *J. Mater. Chem.*, 2011, **21**, 12309.
31 Y. X. Lu, H. Q. Cao, S. C. Zhang and X. R. Zhang, *J. Mater. Chem.*, 2011, **21**, 8633.
32 J. Zhao, M. R. Li, J. L. Sun, L. F. Liu, P. P. Su, Q. H. Yang and C. Li, *Chem.–Eur. J.*, 2012, **18**, 3163.
33 P. Mahata, D. Sarma, C. Madhu, A. Sundaresen and S. Natarajan, *Dalton Trans.*, 2011, **40**, 1952.
34 P. Mahata, T. Aarthi, G. Madras and S. Natarajan, *J. Phys. Chem. C*, 2007, **111**, 1665.
35 J. Zhao, F. Q. Wang, P. P. Su, M. R. Li, J. Chen, Q. H. Yang and C. Li, *J. Mater. Chem.*, 2012, **22**, 13328.